AIP | Review of Scientific Instruments

In situ granular charge measurement by free-fall videography

S. R. Waitukaitis and H. M. Jaeger

Citation: Rev. Sci. Instrum. **84**, 025104 (2013); doi: 10.1063/1.4789496
View online: http://dx.doi.org/10.1063/1.4789496
View Table of Contents: http://rsi.aip.org/resource/1/RSINAK/v84/i2
Published by the American Institute of Physics.

In situ granular charge measurement by free-fall videography

S. R. Waitukaitis and H. M. Jaeger
Department of Physics, The University of Chicago, 5720 S. Ellis Ave, Chicago, Illinois 60637, USA and The James Franck Institute, 929 E 57th Street, Chicago, Illinois 60637, USA

(Received 1 December 2012; accepted 14 January 2013; published online 7 February 2013)

We present the design and performance characterization of a new experimental technique for measuring individual particle charges in large ensembles of macroscopic grains. The measurement principle is qualitatively similar to that used in determining the elementary charge by Millikan in that it follows individual particle trajectories. However, by taking advantage of new technology we are able to work with macroscopic grains and achieve several orders of magnitude better resolution in charge to mass ratios. By observing freely falling grains accelerated in a horizontal electric field with a co-falling, high-speed video camera, we dramatically increase particle tracking time and measurement precision. Keeping the granular medium under vacuum, we eliminate air drag, leaving the electrostatic force as the primary source of particle accelerations in the co-moving frame. Because the technique is based on direct imaging, we can distinguish between different particle types during the experiment, opening up the possibility of studying charge transfer processes between different particle species. For the $\sim$300 μm diameter grains reported here, we achieve an average acceleration resolution of $\sim$0.008 m/s^2, a force resolution of $\sim$500 pN, and a median charge resolution $\sim 6\times 10^4$ elementary charges per grain (corresponding to surface charge densities $\sim$1 elementary charges per μm^2). The primary source of error is indeterminacy in the grain mass, but with higher resolution cameras and better optics this can be further improved. The high degree of resolution and the ability to visually identify particles of different species or sizes with direct imaging make this a powerful new tool to characterize charging processes in granular media. © *2013 American Institute of Physics*. [http://dx.doi.org/10.1063/1.4789496]

I. INTRODUCTION

The electrostatic charging of granular systems plays an important role in a wide variety of contexts. In nature, grain charging can affect the dynamics of dust storms[1–5] and lead to dramatic displays of lightning in volcanic plumes.[6–8] During the industrial handling of grains, spark discharge from ionized grains can lead to catastrophic silo explosions,[9] and electrostatically induced coagulation can undermine the efficient operation of gas fluidized beds and risers.[10] Great care is taken in high tech fabrication processes to prevent contamination from electrostatically charged dust that can ruin sensitive electronic equipment.[11–13] However, despite the relevance of grain charging in so many settings, few experimental techniques are available for making detailed measurements of individual grain charges, and those that are available typically cannot give the precise information necessary to inform why grains charge as they do. Consequently, little is known regarding how grains charge or how charging can be effectively controlled.

The most common techniques give only the most basic information about grain charge or are only applicable to a particular spectrum of grain types. For example, collecting a bulk sample of grains in a Faraday cup, by far the most common technique, only gives access to the net charge of the sample with no information about the particle charge distribution.[14–17] In the handful of variations that do deal with individual grains, the quantity measured is often the charge to mass ratio[18] or a proxy for charge such as the current signal produced in an induction probe.[19,20] There are at least three experiments that use Faraday cup-like devices to measure the absolute charge of individual grains,[21–23] while others such as the E-SPART technique described in Mazumdar *et al.*,[24] which is also capable of measuring the particles' aerodynamic radii, use different variations still.[24] Even so, most of these techniques are restricted to very specific particle sizes, cannot distinguish between different particle compositions, or taint the measurement signal by contributing to the charge being measured.

The technique described here gives direct access to the charge of individual grains, allowing us to quickly construct the full particle charge distribution of a large granular ensemble. The methodology is similar to the original technique developed by Millikan[25] to determine the elementary charge e. As with that experiment, we follow the trajectories of particles in a uniform electric field. However, rather than utilizing the competition between electrostatic forces with air-induced drag and gravity, we instead eliminate drag and gravity to render the electric force as the *only* source of particle accelerations. The technique can be applied to a wide spectrum of grain types and sizes, including systems comprised of two or more separate species, opening the door to detailed study of the mechanics of charge transfer in granular media.

II. EXPERIMENTAL SETUP

A schematic of the apparatus is shown in Fig. 1. A 15 cm diameter, 3.0 m tall acrylic chamber is pumped down to a pressure of 3 mTorr via a turbopump with backing scroll

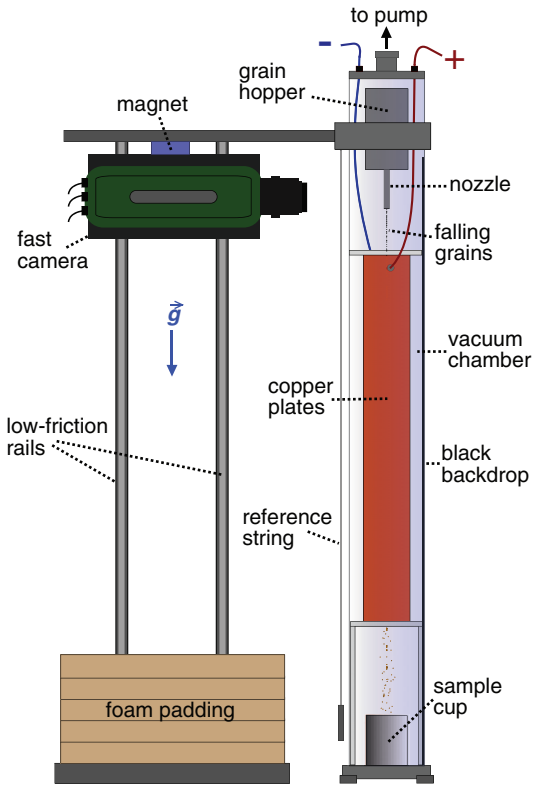

FIG. 1. The experimental setup. Grains freely fall inside a vacuum chamber from the hopper/nozzle through a region between two parallel copper plates held at a potential difference V ($\vec{E}$ points into the page). A camera connected to a carriage-rail system falls with the grains while simultaneously recording video. A vertical reference string hangs in front of the chamber to correct for camera yaw and roll.

pump (a wire mesh filter with holes smaller than the particle diameter prevents grain backflow into the pumps). The top of the chamber houses an aluminum hopper containing the granular material, typically 0.25 kg of grains with diameters d ranging between 100 and 500 μm. The grains are pulled by gravity into a 20 cm long, 2 cm diameter aluminum nozzle. The grains exit the bottom of the nozzle through two apertures of diameter $D \approx 15\bar{d}$. The ratio $D/\bar{d}$ is chosen to be large enough to prevent blockage from granular arching,[26–29] but small enough to avoid the granular droplet formation observed for larger aperture diameters.[30–33] As a result, the grains come out as a dilute stream of individual particles. To prevent unwanted device-grain tribocharging, we pre-coat the interiors of both the hopper and nozzle with the granular material being investigated. (We verify this mitigates charging by running the sample through the nozzle/hopper in atmosphere and measuring the net charge with a Faraday cup; this reveals a mean particle charge $\sim 10^3$ times smaller than the upper charge limit set by the dielectric strength of air, as discussed in McCarty *et al.*[21]).

After opening a mechanical shutter at the bottom of the nozzle, the grains fall freely from the apertures. Approximately 25 cm below, they enter a region between two parallel copper plates (11.5 cm deep × 1.6 mm wide × 1.2 m tall) with a separation of $L = 5.08$ cm. A potential difference V is maintained between the plates with a high-voltage power supply, creating an electric field (pointing into the page in Fig. 1) of strength $|\vec{E}| = V/L$. Outside the chamber, a high-speed camera (Phantom v9.1, 1000 frames per second) is mounted to a carriage that slides freely along two vertical rails. The carriage also houses three high-intensity DC lamps (Dedolight DLH4, not shown in Fig. 1) to illuminate the particles and create contrast between them and the black felt background on the backside of the chamber (backlighting could be employed for dark particles). As the weak coupling between the carriage and the rails leaves the camera vulnerable to slight yaw and roll as it falls, we hang a thin, white, nylon string just outside the chamber to create a vertical reference line. The camera is originally held fixed at the height of the nozzle with an electro-magnet. After the mechanical shutter is opened, the magnet is deactivated and the camera is allowed to fall freely with the grains while simultaneously recording video. At the bottom of the setup, the camera is decelerated by a stack of foam cushions.

For a variety of reasons, it is important that the chamber pressure is maintained below about 10 mTorr. First, the grains and the camera must fall at closely matched speeds throughout the experiment so that we can measure particle trajectories for a sufficiently long time. Although it is easy to increase the camera's terminal velocity in atmospheric pressure by simply adding more weight to the carriage, the only way to ensure the grains are accelerated freely by gravity is by reducing air drag in the chamber. Second, as the dielectric strength of air exhibits a minimum at ∼1 Torr, we must operate at pressures significantly lower than this to avoid dielectric breakdown between the plates. Although we have to pump down through this minimum to reach the operating pressure, this does not seem to lead to corona discharge from the particles. (This is also verified by the Faraday cup measurements, which show the mean charge measured in atmosphere to be close to the mean charge measured in the chamber.) Most importantly, we require that the only significant contribution to the horizontal force acting on the particles is from the electric field. With the chamber at 3 mTorr and the $\bar{d} = 300$ μm grains used in the experiments described here, we limit the effect of residual air drag to be no more than ∼5 pN, which puts the error introduced by drag far below the error associated with imprecision in particle positions.[34]

III. DATA AND ANALYSIS

A. Particle identification and tracking

A portion of a color-inverted still extracted from the high-speed video is shown in Fig. 2(a) (note the full-size images are five times taller and two times wider than this clipping). Fused zirconium dioxide-silicate grains (GlennMills, heterogeneous composite with ZrO_2:SiO_2 ∼ 65:35) appear as soft-black circles in front of the white backdrop (without inversion the particles are white and the background is black). The fuzzy black line extending vertically through the image is the nylon string, which is out of focus as a result of sitting ∼10 cm in front of the grains. The thin white line plotted atop the string is its calculated center position (after yaw and roll corrections). The black circles around most of the particles represent positive particle identifications from the

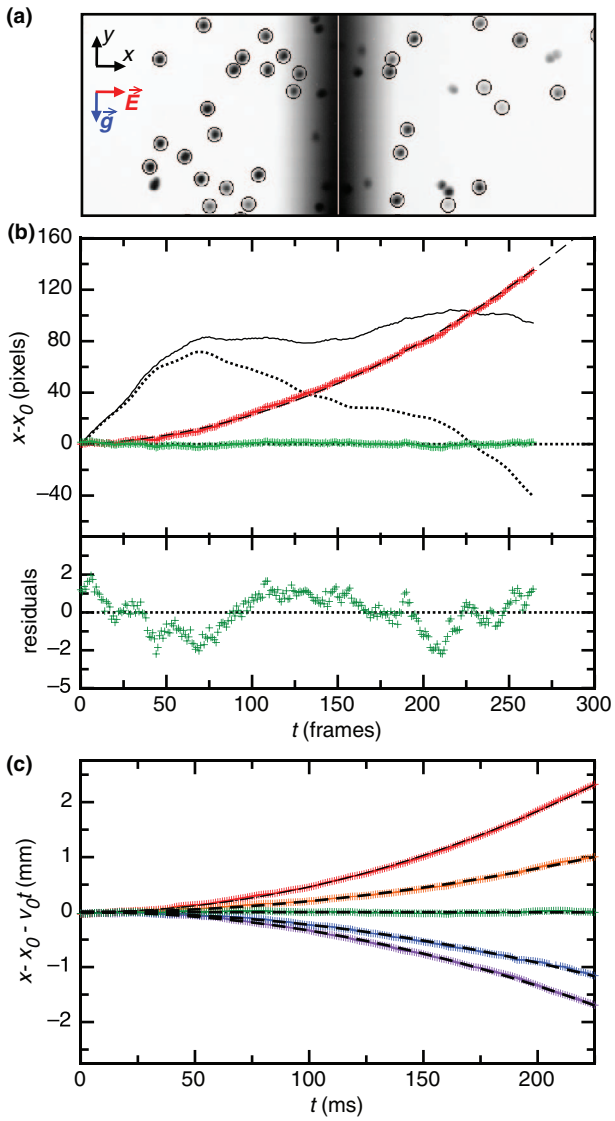

FIG. 2. Particle tracking. (a) Color-inverted still from experiment. Circled particles are positive particle identifications, while the few remaining particles are rejected on basis of size, shape, proximity to the string, or being far out of focus. The fuzzy vertical black strip is the string, and the thin white line is its calculated center position. (b) Example uncorrected particle position (black line), string position (dotted black line), and corrected particle position (red points) vs. time (particle and string are measured relative to their initial positions). The green data are the residuals from fitting the corrected trajectory to a parabola, which have a rms deviation of ∼0.5 pixels. (c) Sampling of the corrected horizontal deflection (i.e., $x - v_0 t - x_0$) for a few particles of different charges at $V = 2250$ V ($|\vec{E}| = 44300$ V/m).

particle-tracking algorithm (IDL code developed by Crocker and Grier[35]). The code has been tuned to neglect particle clusters (extraordinarily large or highly elliptical features), out of focus particles (features that are too dim), and particles that are too close to the string center.

We are able to reconstruct trajectories that last 20 frames or more (0.02 s) for about 90% of the particles in the field of view. A typical uncorrected horizontal trajectory is shown in Fig. 2(b). The yaw and roll of the camera, though subtle, introduce significant perceived motion of the particles, making their trajectories appear rather unpredictable. However, the horizontal trajectory of the string is subject to the same artifacts and can therefore be used to correct for this. After subtracting the string's center position from the particle position, we recover a clean trajectory, and by fitting this curve to a parabola we extract a measurement for the particle acceleration a (as well as the initial position x_0 and velocity v_0). The root mean squared residuals from these fits (Fig. 2(b)) are on the order of 0.5 pixels. As the lifetime τ (i.e., the total time a particle remains in the field of view) varies from one grain to another, the error in the measured accelerations σ_a is different for each grain, with lower σ_a for longer τ. On average, however, we find $\bar{\sigma}_a \approx 8 \times 10^{-3}$ m/s^2, largely independent of plate voltage V (see Fig. 4(b)).

B. Trajectory filtering

As the grains fall and are accelerated by the field, it is not uncommon for them to collide or cross paths. These events can significantly alter a grain's trajectory and give rise to spurious acceleration calculations if the videos are batch-processed and these events go unflagged. An example of such an event is shown in Fig. 3(a), where we plot the trajectory for a grain that has undergone a path-changing collision that yields a perceived acceleration ∼0.5 m/s^2. We identify and reject these particles by plotting the acceleration errors σ_a vs. the lifetimes τ, as in Fig. 3(b). Most tracks fall in a clear band

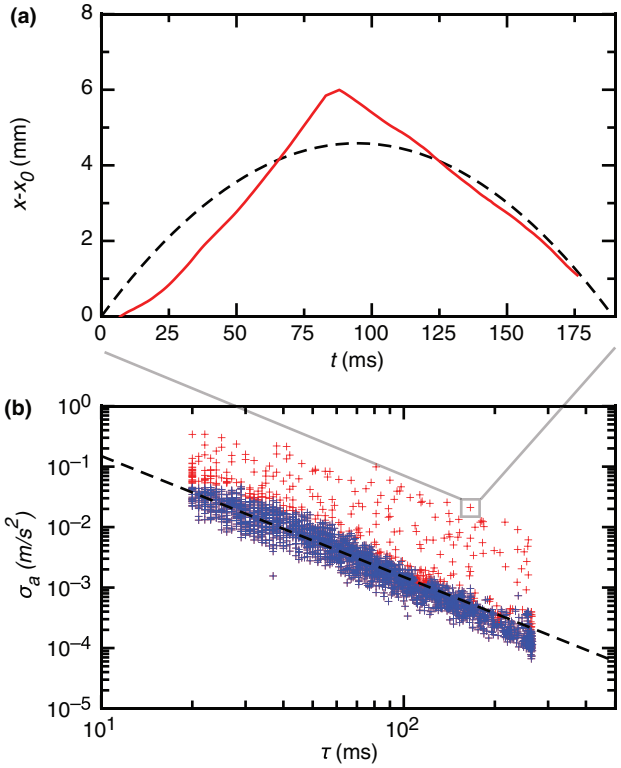

FIG. 3. Filtering procedure to reject colliding and crossing particles. (a) Example particle trajectory ($x - x_0$ vs. t) of a particle involved in a collision/crossing. The event leads to a perceived acceleration of ∼0.5 m/s^2, although it is clear from either leg of the trajectory that the actual acceleration is much smaller than this. (b) Errors on acceleration fits σ_a vs. particle lifetime τ. Most measurements (blue data) fall into a band $\sigma_a \propto \tau^{-2}$, while the colliding/crossing particles lie above this trend. These tracks (red data) are rejected by binning along τ, finding the average σ_a in each bin by fitting to a Gaussian, and then rejecting particles whose σ_a lies three sigma above their bin mean.

of points consistent with $\sigma_a \propto \tau^{-2}$, but a spattering of rogue values persists above this. These data correspond to the colliding or crossing particles. To reject these data, we bin the particles along τ, find the average σ_a in each bin by fitting to a Gaussian, and then exclude those particles whose acceleration error lies three sigma above their bin mean. This step typically results in a rejection of ~10% of the original particle population.

C. Relating accelerations to charges

After collecting data for several (typically 20) movies, analyzing the resulting $\sim 10^4$ trajectories, and filtering the results as described above, we are able to reconstruct the full particle acceleration distribution $P(a)$ for the granular material. Examples are shown in Fig. 4(a) for different voltages V. As the acceleration errors σ_a are different for each particle tracked and vary by nearly two orders of magnitude, we make these distributions by weighting each track by its error $w = 1/\sigma_a^2$. As we expect, increased plate voltage leads to broader distributions and slightly shifted centroids. We quantify this in Fig. 4(b), where we plot the mean acceleration $\bar{a}$ (weighted by $w = 1/\sigma_a^2$) and the width Δ_a (rms deviation from the mean, also weighted by $w = 1/\sigma_a^2$) as a function of plate voltage V. For a particle charge distribution $P(q)$ with mean charge $\bar{q}$, we expect the mean acceleration $\bar{a}$ to be given by

$$\bar{a} = s_a V = \frac{\bar{q} V}{L \bar{m}}, \tag{1}$$

i.e., a linear relationship whose slope is given by $s_a = \bar{q}/L\bar{m}$ ($\bar{m}$ is the average particle mass). For the distribution widths, we expect the relationship:

$$\Delta_a = \sqrt{\Delta_0^2 + (s_\Delta V)^2} = \sqrt{\Delta_0^2 + \left(\frac{\Delta_q V}{L\bar{m}}\right)^2}, \tag{2}$$

where Δ_0 is the error baseline for an acceleration measurement and $s_\Delta = \Delta_q V/L\bar{m}$ is the slope of the Δ_a vs. V curve for $\Delta_a \gg \Delta_0$. The dashed lines in Fig. 4(b) are fits to these equations for the width and mean, where we find $s_a = -(3.2 \pm 0.6) \times 10^{-6}$ (m/s^2)/V, $\Delta_0 = (8.5 \pm 0.3) \times 10^{-3}$ m/s^2, and $s_\Delta = (2.6 \pm 0.5) \times 10^{-5}$ (m/s^2)/V. As one would expect, the width Δ_0 is nearly the same as the average error in our individual acceleration measurements ($\bar{\sigma}_a = (8 \pm 1) \times 10^{-3}$ m/s^2). The correspondence between the fits and the data confirms the methodology, but it also reveals that our dilute, freely falling granular stream is unaffected by the field-induced dipole charging encountered in dense granular systems.[36]

The final step in the measurement process is to relate the fitted parameters s_a and s_Δ to the mean charge $\bar{q}$ and charge width Δ_q. To do this, we only need to know the average particle mass $\bar{m}$. We can in principle extract a rough measure of this quantity by directly measuring particle sizes from the videos. While the spatial resolution of our imaging (our 1640 × 1200 pixel camera and 200 mm macro lens achieves ~12.5 μm/pixel) is good enough to resolve a binary particle size distribution $P(d)$ of sufficiently differently sized particles, is not sufficiently good to resolve slight size differences in highly monodisperse samples. Here, we take advantage of the non-invasive nature of our experiment and simply collect the grains at the bottom of the chamber and size them in an optical microscope afterwards. Figure 4(c) shows $P(d)$ for the sample, which has a mean particle diameter $\bar{d} = 300 \pm 9$ μm.

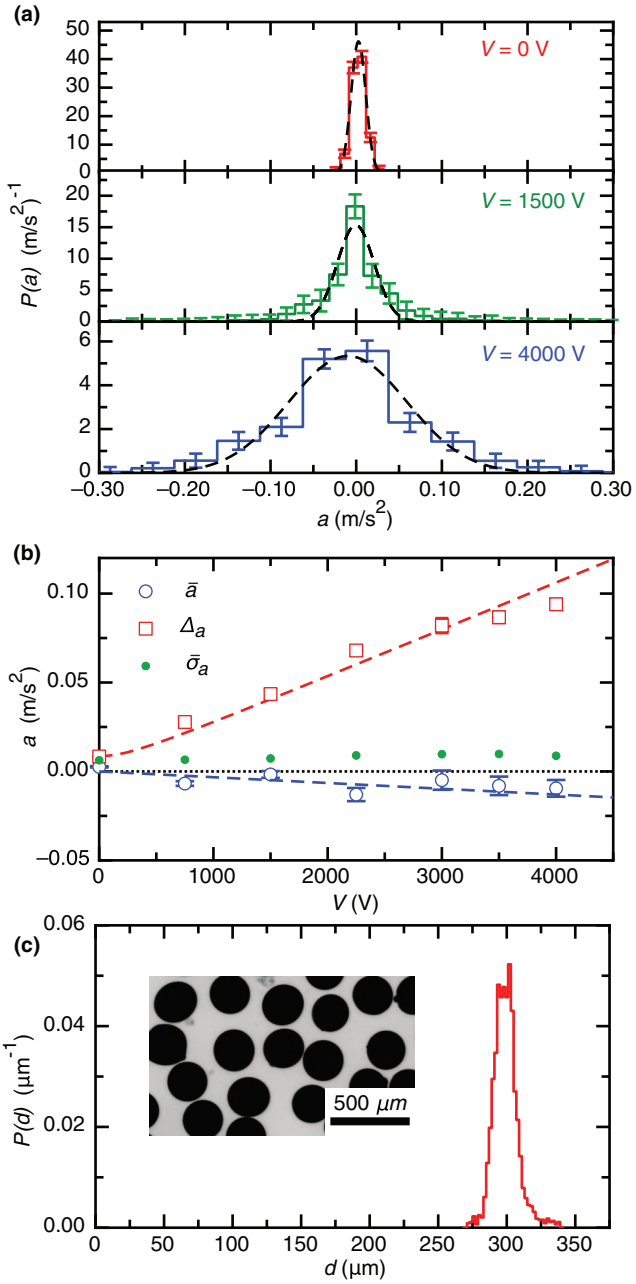

FIG. 4. Relating acceleration distributions to charge measurements. (a) Particle acceleration distributions $P(a)$ (weighted by $w = 1/\sigma_a^2$) for voltages V =0, 1500, and 4000 V ($|\vec{E}| = 0$, 30 000, and 79 000 V/m, respectively). (b) Change in distribution width Δ_a (red squares), mean $\bar{a}$ (blue circles), and mean acceleration error $\bar{\sigma}_a$ (green dots) vs. V. Calculations for Δ_a and $\bar{a}$ are also weighted by $w = 1/\sigma_a^2$, and the error bars are the standard deviations as calculated from $N = 1000$ bootstrap resamples of the original measurement population. Dashed line fits for $\bar{a}$ and Δ_a correspond to Eqs. (1) and (2), respectively. (c) Particle size distribution $P(d)$ as calculated from imaging particles with optical microscope. Inset: microscope image (color inverted). Using these data to calculate the mean diameter $\bar{d}$ and particle mass $\bar{m}$, we can use Eqs. (1) and (2) to calculate the mean charge $\bar{q} = -(6 \pm 1) \times 10^4$ e and width $\Delta_q = (4.5 \pm 0.4) \times 10^5$ e of the particle charge distribution.

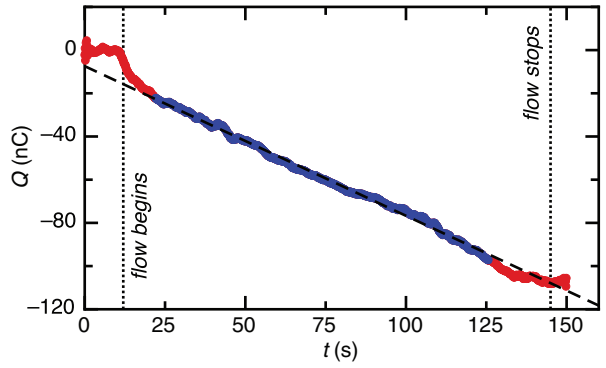

FIG. 5. Independent measure of average charge per particle $\bar{q}$ with Faraday cup. Plot of total charge in cup Q vs. time t. Data are smoothed to remove 60 Hz noise (∼10 nC peak to peak). We calculate the charge flow rate dQ/dt and mass flow rate dM/dt from this graph.

This corresponds to a mean particle mass $\bar{m} = (54 \pm 5) \times 10^{-9}$ kg. Using this mean mass with the parameters s_a and s_Δ extracted from the fits in Fig. 4(b), we find that the grains investigated here have a mean charge $\bar{q} = (-6 \pm 1) \times 10^4\ e$ and a charge width $\Delta_q = (4.5 \pm 0.4) \times 10^5\ e$ (where we take e to be the magnitude of the electron charge).

As a validation measure, we can crosscheck the result for the mean charge $\bar{q}$ by collecting the sample in a Faraday cup. We typically do this before putting the grains in the chamber by letting them slowly flow from the same hopper/nozzle into the guarded Faraday cup while a Keithley 6514 electrometer records the total charge in the cup, $Q(t)$. Figure 5 shows the result for the sample here. After an abrupt initial jump as the grains just begin to flow, the total accumulated charge grows linearly with time until the flow stops. From this we can measure the charge flow rate dQ/dt (by fitting a line to the central portion of the graph) and the mass flow rate dM/dt (by dividing the total mass M by the total flow time as indicated in the figure). With our knowledge of the particle mass $\bar{m}$ from the microscope images, we can calculate the average particle charge via

$$\bar{q} = \frac{dQ}{dt}\frac{dt}{dM}\bar{m}. \tag{3}$$

With this measurement (Fig. 5), we find that $\bar{q} = (-8.7 \pm 0.8) \times 10^4\ e$, very close to but slightly more negative than what we find from measuring and analyzing the full particle charge distribution with the freefall apparatus.

IV. CONCLUSIONS

We have constructed and characterized an experimental system capable of measuring the electric charge of individual grains with high precision. Unlike other systems that only measure the charge to mass ratio, our system allows us to measure the absolute charge of individual specimens in a large ensemble of grains, giving access to the full particle charge distribution. Our measurement is non-invasive in that it does not affect the charge of the grains being measured and in that it allows us to salvage potentially precious samples after each experiment. Being based on direct observation of particles, we can measure charge distributions of mixed granular media, opening up the possibility of studying charge transfer arising from differences in grain chemistry or size. With the granular media and setup as discussed here, we achieve a median charge resolution of $6 \times 10^4\ e$, with the primary contribution to the error being the uncertainty in the particle mass. While this is the highest resolution measurement reported so far, the system is capable of performing even better with straightforward improvements. Higher resolution imaging, for example, could allow one to precisely determine the particle size distribution *in situ* and thus reduce the error introduced by uncertainty in the mass. The technique as described allows us to determine a detailed charge distribution for a sample in a day, but it is easy to envision automating the system to run more efficiently and for longer periods of time to create ultra-refined charge distributions. These possibilities open the door to using this technique as a way to probe the subtle dynamics of charge transfer in granular media.

ACKNOWLEDGMENTS

The authors gratefully acknowledge the contributions to the project made by Gustavo Castillo, Estefania Vidal, Suomi Ponce Heredia, and Alison Koser. We benefited a great deal from discussions with Dan Lacks, Troy Shinbrot, Ray Cocco, and Ted Knowlton. We thank Mrs. Joan Winstein for her recognition and support. This work was supported financially by the National Science Foundation (NSF) through its Materials Research Science and Engineering Center (MRSEC) program (DMR-0820054) and by the US Army Research Office through Grant No. W911NF-12-1-0182. S.R.W. acknowledges support from a University of Chicago Millikan Fellowship.

[1] J. R. Leeman and E. D. Schmitter, "Electric signals generated by tornados," Atmos. Res. **92**, 277 (2009).
[2] G. Freier, "The electric field of a large dust devil," J. Geophys. Res. **65**, 3504, doi:10.1029/JZ065i010p03504 (1960).
[3] O. Melnik and M. Parrot, "Electrostatic discharge in Martian dust storms," J. Geophys. Res. **103**, 29107, doi:10.1029/98JA01954 (1998).
[4] J. Kok and N. Renno, "Electrostatics in wind-blown sand," Phys. Rev. Lett. **100**, 014501 (2008).
[5] D. Schmidt, R. Schmidt, and J. Dent, "Electrostatic force on saltating sand," J. Geophys. Res. **103**, 8997, doi:10.1029/98JD00278 (1998).
[6] M. Brook, C. Moore, and T. Sigurgeirsson, "Lightning in volcanic clouds," J. Geophys. Res. **79**, 472, doi:10.1029/JC079i003p00472 (1974).
[7] R. Anderson, S. Gathman, J. Hughes, S. Bjornsson, S. Jonasson, D. Blanchard, C. Moore, H. Survilas, and B. Vonnegut, "Electricity in volcanic clouds: Investigations show that lightning can result from charge-separation processes in a volcanic crater," Science **148**, 1179 (1965).
[8] T. Mather and R. Harrison, "Electrification of volcanic plumes," Surv. Geophys. **27**, 387 (2006).
[9] D. Thorpe, S. Singh, P. Cartwright, and A. Bailey, "Electrostatic hazards in sugar dust in storage silos," J. Electrostat. **16**, 193 (1985).
[10] R. Cocco, F. Shaffer, R. Hays, S. B. R. Karri, and T. Knowlton, "Particle clusters in and above fluidized beds," Powder Technol. **203**, 3 (2010).
[11] A. C. K. Lai, S. C. M. Yu, and F. Chen, "Convective diffusion of particles deposition under electrostatics from turbulently-mixed conditions," Chem. Eng. Sci. **59**, 2929 (2004).
[12] S. Kim and C. J. Lawrence, "Suspension mechanics for particle contamination control," Chem. Eng. Sci. **43**, 991 (1988).
[13] H. H. Schicht, "Contamination control—An indispensable factor in high-technology manufacturing tasks," J. Aerosol Sci. **21**, S719 (1990).
[14] K. R. Lamarche, X. Liu, S. K. Shah, T. Shinbrot, and B. J. Glasser, "Electrostatic charging during the flow of grains from a cylinder," Powder Technol. **195**, 158 (2009).

[15]A. Mehrotra, F. J. Muzzio, and T. Shinbrot, "Spontaneous separation of charged grains," Phys. Rev. Lett. **99**, 058001 (2007).
[16]A. Sowinski, F. Salama, and P. Mehrani, "New technique for electrostatic charge measurement in gas-solid fluidized beds," J. Electrostat. **67**, 568 (2009).
[17]D. A. Engers, M. N. Fricke, A. W. Newman, and K. R. Morris, "Triboelectric charging and dielectric properties of pharmaceutically relevant mixtures," J. Electrostat. **65**, 571 (2007).
[18]F. Ali, M. Ali, R. Ali, and I. Inculet, "Minority charge separation in falling particles with bipolar charge," J. Electrostat. **45**, 139 (1998).
[19]K. M. Forward, D. J. Lacks, and R. M. Sankaran, "Methodology for studying particle-particle triboelectrification in granular materials," J. Electrostat. **67**, 178 (2009).
[20]S. S. Kausik, M. Chakraborty, P. Dutta, M. Kakati, and B. K. Saikia, "Study of charge distribution in a dust beam using a Faraday cup," Phys. Lett. A **372**, 860 (2008).
[21]L. S. McCarty, A. Winkleman, and G. M. Whitesides, "Ionic electrets: Electrostatic charging of surfaces by transferring mobile ions upon contact," J. Am. Chem. Soc. **129**, 4075 (2007).
[22]W. Hu, L. Xie, and X. Zheng, "Contact charging of silica glass particles in a single collision," Appl. Phys. Lett. **101**, 114107 (2012).
[23]T. Sickafoose, J. Colwell, M. Horányl, and S. Robertson, "Photoelectric charging of dust particles in vacuum," Phys. Rev. Lett. **84**, 6034 (2000).
[24]M. Mazumdar, R. Ware, T. Yokoyama, B. Rubin, and D. Kamp, "Measurement of particle size and electrostatic charge distributions on toners using e-spart analyzer," IEEE Trans. Ind. Appl. **27**, 611 (1991).
[25]R. A. Millikan, "On the elementary electrical charge and the Avogadro constant," Phys. Rev. **32**, 349 (1911).
[26]K. To, P.-Y. Lai, and H. Pak, "Jamming of granular flow in a two-dimensional Hopper," Phys. Rev. Lett. **86**, 71 (2001).
[27]K. To, P.-Y. Lai, and H. K. Pak, "Flow and jam of granular particles in a two-dimensional hopper," Physica A **315**, 174 (2002).
[28]C. Mankoc, A. Janda, R. Arévalo, J. M. Pastor, I. Zuriguel, A. Garcimartin, and D. Maza, "The flow rate of granular materials through an orifice," Granular Matter **9**, 407 (2007).
[29]W. A. Beverloo, H. A. Leniger, and J. van de Velde, "The flow of granular solids through orifices," Chem. Eng. Sci. **15**, 260 (1961).
[30]M. Möbius, "Clustering instability in a freely falling granular jet," Phys. Rev. E **74**, 051304 (2006).
[31]J. R. Royer, D. J. Evans, L. Oyarte, Q. Guo, E. Kapit, M. E. Möbius, S. R. Waitukaitis, and H. M. Jaeger, "High-speed tracking of rupture and clustering in freely falling granular streams," Nature (London) **459**, 1110 (2009).
[32]S. Waitukaitis, H. Grütjen, J. Royer, and H. Jaeger, "Droplet and cluster formation in freely falling granular streams," Phys. Rev. E **83**, 051302 (2011).
[33]S. Ulrich and A. Zippelius, "Stability of freely falling granular streams," Phys. Rev. Lett. **109**, 166001 (2012).
[34]See supplementary material at http://dx.doi.org/10.1063/1.4789496 for a thorough discussion of residual air drag.
[35]J. C. Crocker and D. G. Grier, "Methods of digital video microscopy for colloidal studies," J. Colloid Interface Sci. **179**, 298 (1996).
[36]T. Pähtz, H. J. Herrmann, and T. Shinbrot, "Why do particle clouds generate electric charges?" Nat. Phys. **6**, 364 (2010).

Supplementary discussion on residual air drag

Scott R. Waitukaitis & Heinrich M. Jaeger
The Department of Physics and
The James Franck Institute at
The University of Chicago
929 E 57th Street, Chicago IL 60612

December 5, 2012

I Air drag

The viscous drag on a particle moving through a gas changes significantly as a function of pressure. For high pressure environments (P_{atm} and higher), this comes as a correction for finite Reynold's number and arises because the gas density scales with the pressure ($\rho = \rho_{atm}P/P_{atm}$). At very low pressures, an entirely different effect works to reduce drag dramatically. This begins to occur when the mean free path of the gas molecules λ becomes larger than the particle diameter d, i.e. for large Knudsen number ($K = 2\lambda/d$). For our system, $\lambda \approx 1.7$ cm, leading to a Knudsen number $K = \lambda/d \approx 115$ ($d = 300$ μm).

This suggests immediately that air drag is highly irrelevant, but since we are doing a precision measurement, we want to make a detailed estimate of exactly how significant it is, since even small amounts could lead to systematic measurement error. We start by modifying Stoke's drag equation $F_S = 3\pi\eta dv$ with a correction for high Knudsen number (i.e. low pressure). This correction is of the form

$$F_d = F_S(1 + K(a + be^{c/K}))^{-1} \approx 0.01F_S, \tag{1}$$

where $a = 0.86$, $b = 0.29$, and $c = 1.25$ are empirical fit parameters taken from the experiment by Milikan [35]. As indicated, the effect of this correction to the normal Stokes drag for the parameters in our system is to make it $\sim$100 times smaller. At the *maximum* vertical speed of the particles ($v_m = \sqrt{2gH} \approx 6.5$ m/s), the drag force is on the order of $F_d \approx 3$ nN, much smaller than the grain weight $mg \approx 53$ nN. Thus, for the vertical motion, the grains are virtually in total free-fall for the entire experiment.

The absence of vertical drag is important for ensuring the grains are in the field of view throughout the fall, but it is the horizontal drag that can contribute to error in the charge measurement. To decide whether or not this is relevant, we must take into consideration a few factors. The first is the horizontal velocity distribution of the particles imprinted on them as they leave the hopper. This is

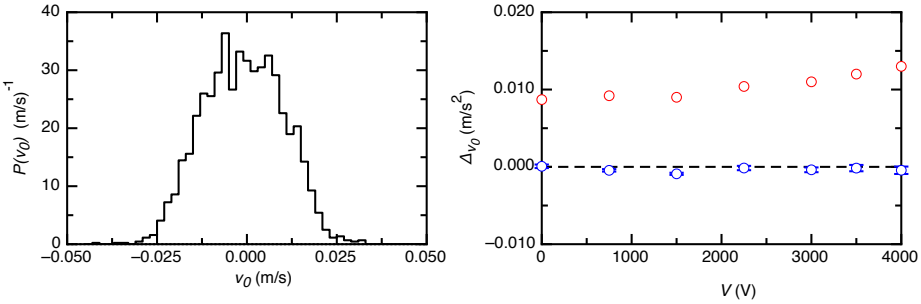

Figure 1: Nozzle-imprinted initial horizontal velocities. (a) Horizontal velocity distribution $P(v_0)$ for $V = 0$ V. (b) $|v_0|$ and Δ_{v_0} as a function of V. The increase in field has little effect on the initial velocity and width, indicating that the fringe field the particles experience before entering the region between the plates has little effect on their trajectories. The typical initial horizontal speed at all V is $\sim$1 cm/s, implying a drag force $F_d \sim$5 pN.

shown in Fig. 1, where we plot the distribution of initial velocities at 0 V as well as the evolution of the mean velocity v_0 and the velocity width Δ_{v_0} vs. V. For all applied field values, the mean v_0 is close to zero and the width is $\sim$1 cm/s. If either of these numbers were particularly large, the horizontal component of the drag could compromise the measurement resolution. At a typical speed of 1 cm/s, however, we only expect a drag force on the order of $\sim$5 pN, indicating that this is not of concern.

A second factor to be considered is whether or not grains that are accelerated to "high" velocities by the field are adversely affected by the increase in drag. Since this varies with each grain, we look at the general equation of motion for any grain, which is given by

$$ma = -F_d + qE. \tag{2}$$

where m is the grain mass, a the acceleration, q the grain's charge, $E = V/L$ is the external electric field, and F_d the drag law given in Eq. 1. The solutions to Eq. 2 are of course exponential in time, with a grain's horizontal speed asymptotically approaching the value $|v_f| = qE/k$ with time constant $\tau_{drag} = m/k$. One way to examine whether or not drag is important as particles are accelerated to higher and higher velocities is by comparing the timescale τ_{drag} to the time during which the grains are between the plates ($\Delta t \sim 0.26$ s). For the parameters in our experiment, $\tau_{drag}/\Delta t \approx 110/0.26$. This indicates that particles will have trajectories whose equations of motion are well-approximated by $ma = qE$. More quantitatively still, we can estimate the scale of error this introduces to an acceleration fit by solving Eq. 2 and expanding the solution to second order:

$$x(t) = x_0 + (v_f - v_0)\tau_{drag} + v_0 t + \frac{v_f - v_0}{2\tau_{drag}} t^2. \tag{3}$$

The term $v_f/2\tau$ is just the external acceleration qE/m, and the term subtracted from it $v_0/2\tau$ is the error introduced to the acceleration from the viscous drag (note the drag leads to smaller perceived accelerations). Directly evaluating this term, we find the acceleration errors introduced by drag are on the order of 10^{-4} m/s^2, much smaller than the error baseline we encounter experimentally (i.e. the $\sim$0.008 m/s^2 associated with scatter in the measured particle position and variable lifetime τ).

References

[35] R. Millikan, The general law of fall of a small spherical body through a gas and its bearing upon the nature of molecular reflection from surfaces, Phys. Rev. **22**, 1 (1923).